Supporting Information

Cellulose nanocrystal/halloysite nanotube composite aerogels for water purification

*Huan Gao,[a,b] Miguel A. Soto,[a] Zongzhe Li,[a] Lucas J. Andrew[a] and Mark J. MacLachlan[a,c,d]**

[a] *Department of Chemistry, University of British Columbia, 2036 Main Mall, Vancouver, BC, V6T 1Z1, Canada.*

[b] *School of Chemistry and Materials Science, Nanjing Normal University, Nanjing, 210023, China*

[c] *Stewart Blusson Quantum Matter Institute, University of British Columbia, 2355 East Mall, Vancouver, BC, V6T 1Z4 Canada*

[d] *WPI Nano Life Science Institute, Kanazawa University, Kanazawa, 920-1192, Japan*

Corresponding Author

Mark J. MacLachlan* *E-mail: mmaclach@chem.ubc.ca*

Table of contents for supplementary information

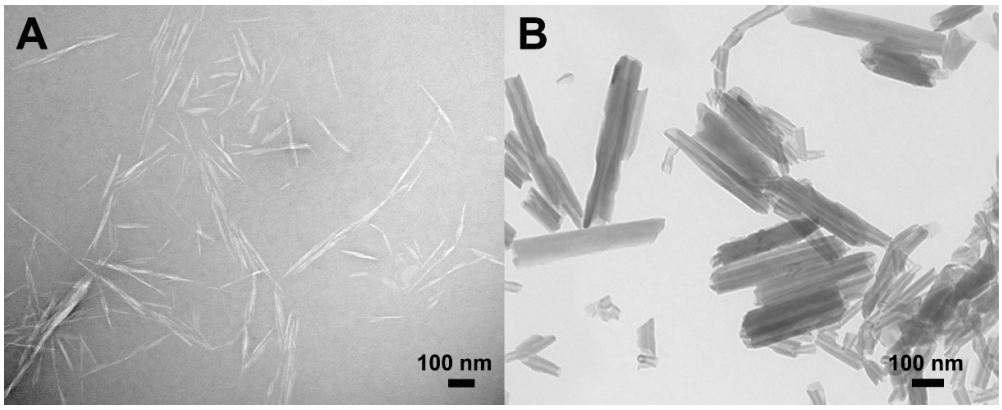

Fig. S1 TEM images of (A) CNCs and (B) HNTs.

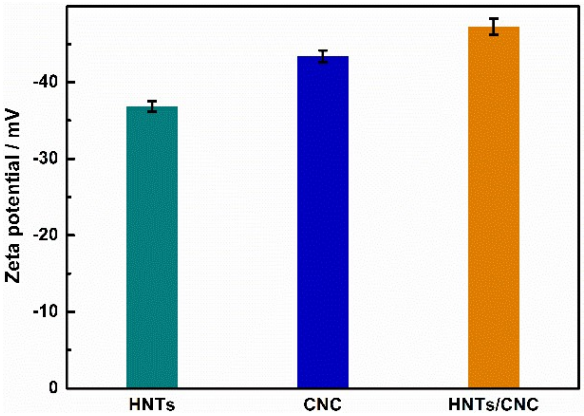

Fig. S2 ζ-potential measurements for HNT, CNC and HNT/CNC suspensions. The error bars represent the standard deviations based on three independent tests of the same sample.

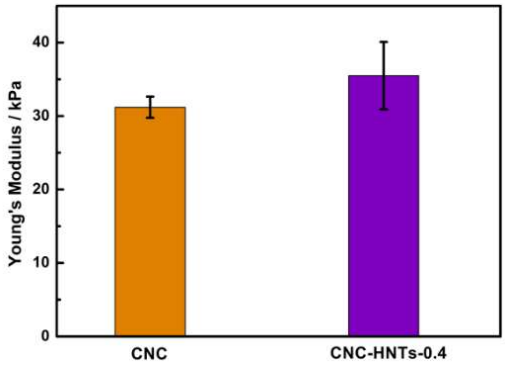

Fig. S3 Young's moduli of CNC aerogel and CNC-HNT-0.4. The error bars represent the standard deviations based on three independent tests of samples with the same composition.

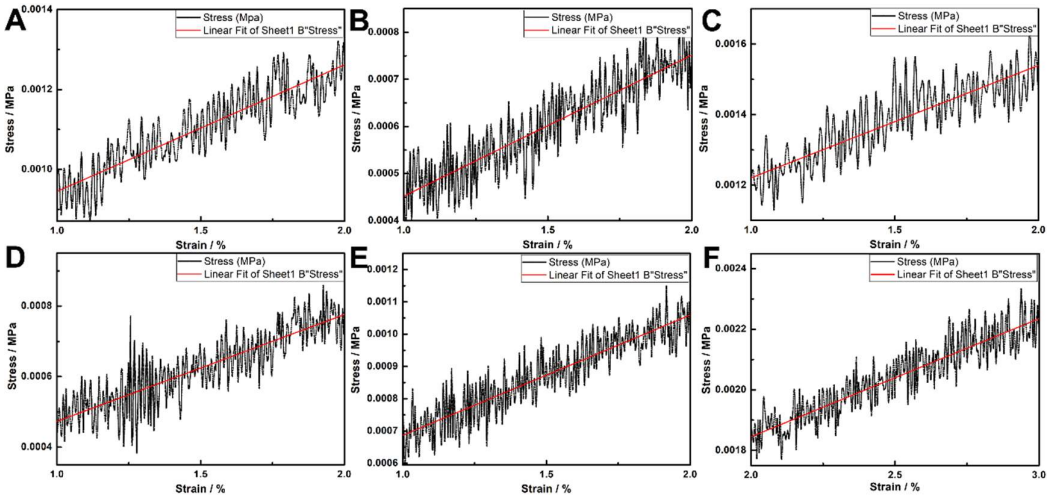

Fig. S4 Compressive stress-strain curves of CNC aerogel (A, B, C; these correspond to three independent samples) and CNC-HNT-0.4 (D, E, F).

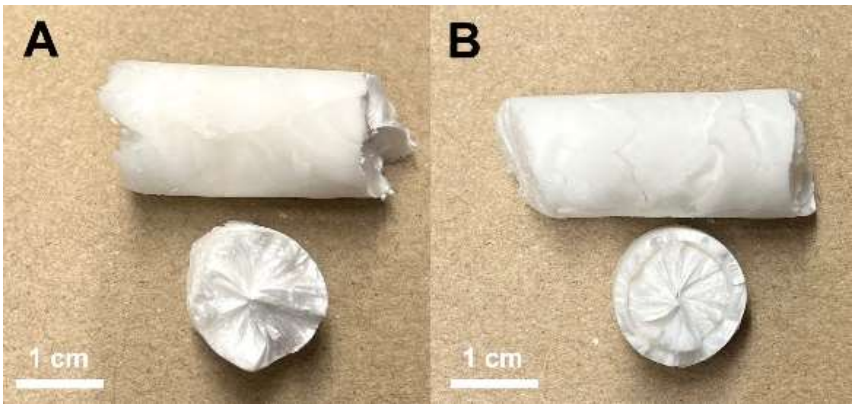

Fig. S5 Photographs of (A) CNC aerogel and (B) CNC-HNT-0.4.

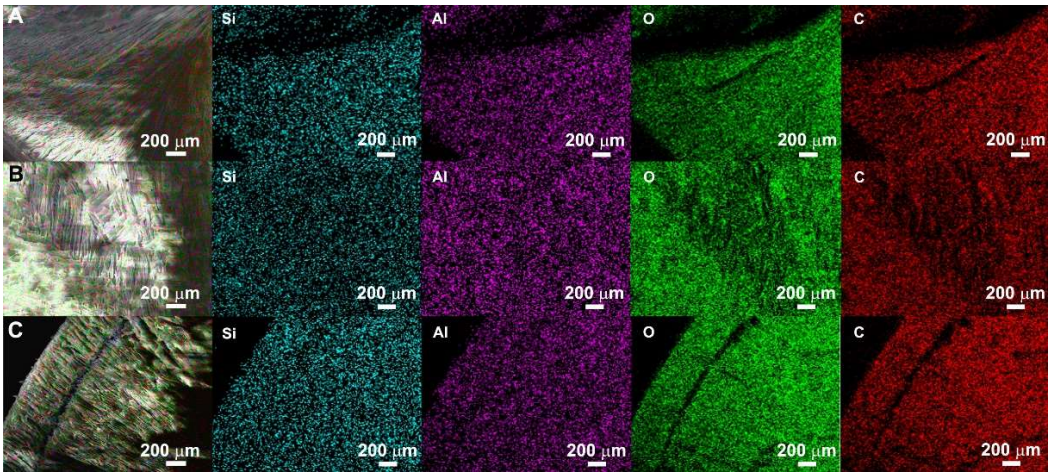

Fig. S6 (A, B and C) SEM-EDX mapping of three different spots on the top of CNC-HNT-0.4.

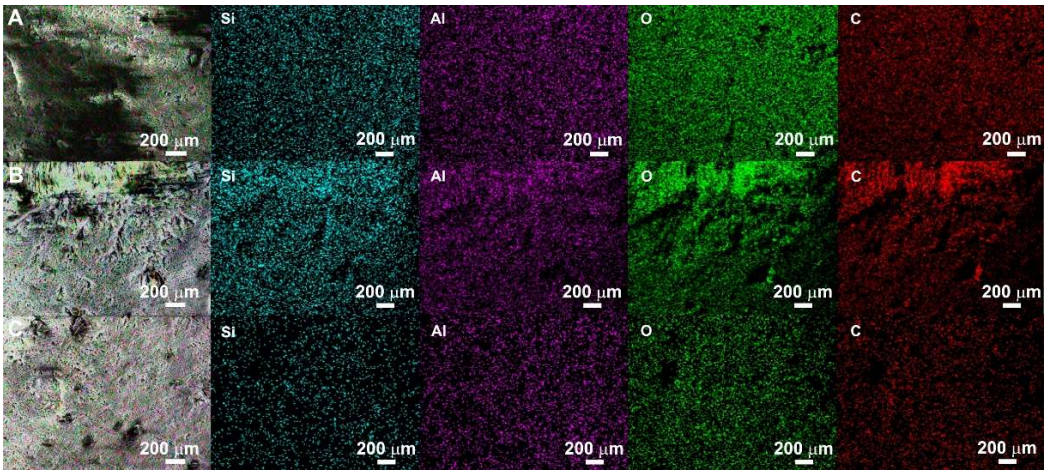

Fig. S7 (A, B and C) SEM-EDX mapping of three different spots on the side of CNC-HNT-0.4.

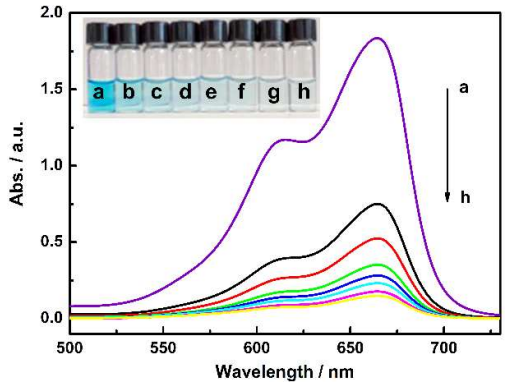

Fig. S8 Initial removal tests using CNC-HNT aerogels. The starting MB solution concentration was 10 mg·L^{-1}. Spectra show absorbance of (a) the initial MB solution (10 mg·L^{-1}) and (b-h) the residual solutions after soption with (b) CNC, (c) CNC-HNT-0.1, (d) CNC-HNT-0.2, (e) CNC-HNT-0.3, (f) CNC-HNT-0.4, (g) CNC-HNT-0.5 and (h) CNC-HNT-0.6 (from b to h). The inset shows photos of (a) the initial MB solution (10 mg·L^{-1}) and (b-h) the corresponding residual solutions after sorption.

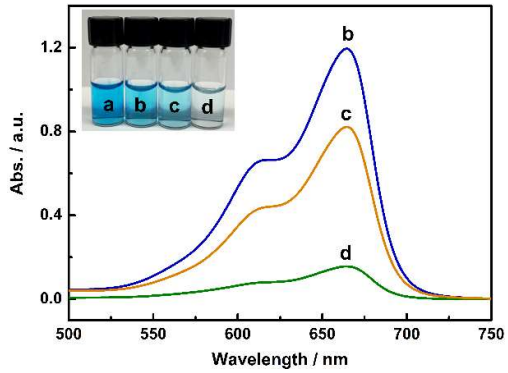

Fig. S9 UV-vis spectra of residual MB in solutions after treatment with (b) HNTs, (c) CNC aerogel and (d) CNC-HNT-0.4. The inset shows photos correspond to (a) the initial MB solution (10 mg·L^{-1}) and (b-d) the corresponding residual solutions after sorption.

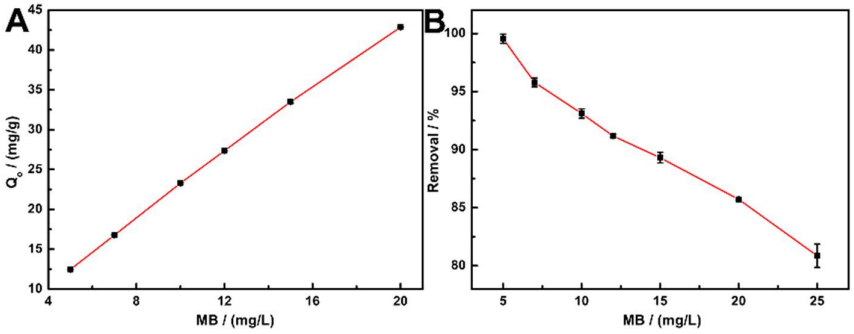

Fig. S10 Effect of initial dye concentration on (A) the adsorption capacity and (B) the removal efficiency of MB. MB concentration 5-20 mg·L^{-1}, CNC-HNT-0.4 4 mg. Error bars are the standard deviations corresponding to three independent experiments.

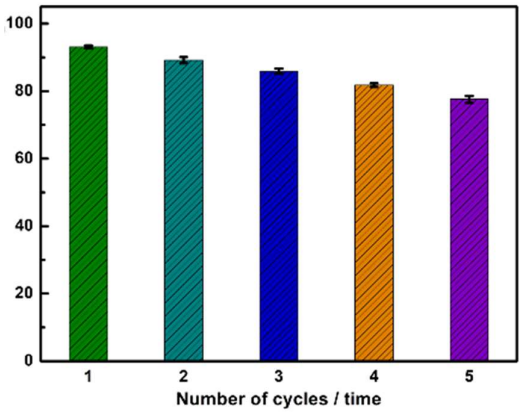

Fig. S11 Reusability of CNC-HNT-0.4 aerogel as MB adsorbent for five successive cycles. Error bars are the standard deviations corresponding to three independent experiments with the same samples.

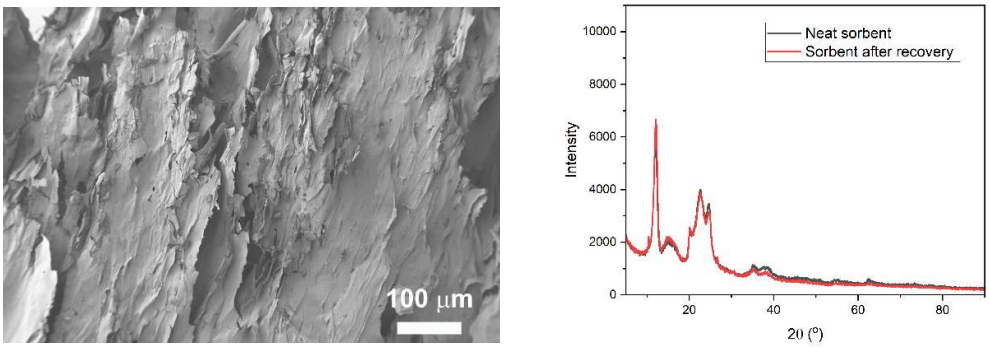

Fig. S12 SEM image (A) and PXRD pattern (B) of CNC-HNT-0.4 sorbents after MB desorption.

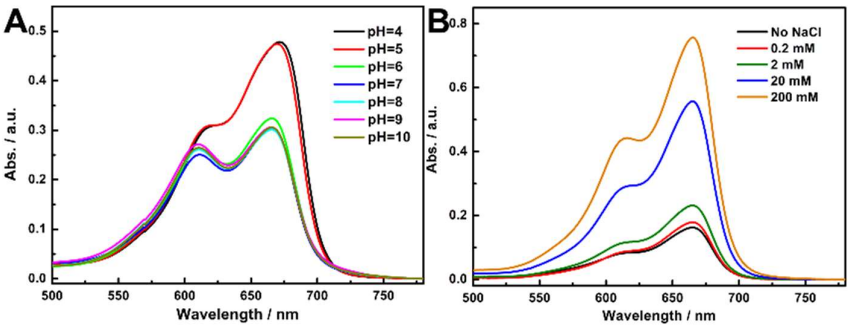

Fig. S13 UV-vis spectra for MB adsorption capacity tests at (A) different pH and (B) different ionic strength. MB concentration 10 mg·L^{-1}, CNC-HNT-0.4 4 mg, equilibration time 360 min, room temperature.

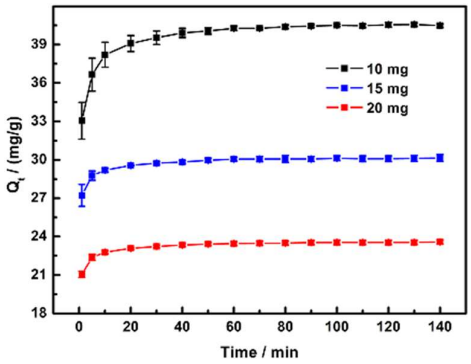

Fig. S14 Adsorption capacity as a function of adsorption time for MB adsorption. CNC-HNT-0.4 10 mg (black), 15 mg (blue) and 20 mg (red); 50 mL solution of MB with a concentration of 10 mg·L^{-1}. Error bars are the standard deviations corresponding to three independent experiments with the same samples.

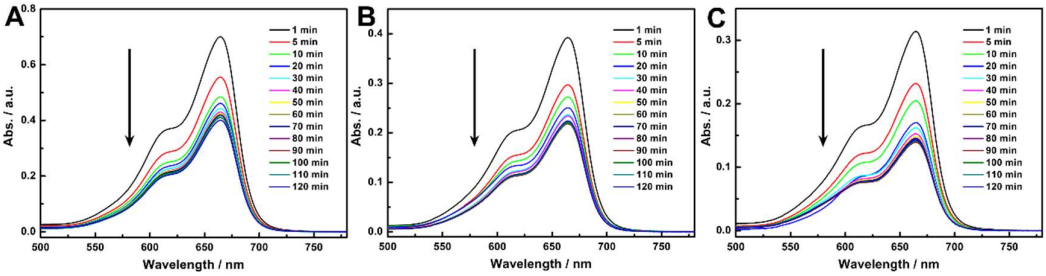

Fig. S15 Successive UV-vis absorption spectra of MB solution in the presence of (A) 10 mg, (B) 15 mg, and (C) 20 mg of CNC-HNT-0.4.

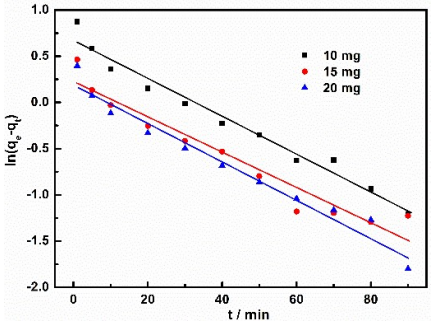

Fig. S16 Data fitting to pseudo-first order kinetic model; CNC-HNT-0.4 aerogel 10 mg (black), 15 mg (red) and 20 mg (blue). The data were collected from three independent experiments.

Table S1. Kinetic parameters obtained from the fitting to a pseudo-first order model.

Adsorbent (mg)	Experimental Q_e ($mg \cdot g^{-1}$)	Pseudo-first order K_1 (min^{-1})	$Q_{e,1}$ ($mg \cdot g^{-1}$)	R^2
10	40.51	0.0474	4.68	0.974
15	30.12	0.0440	1.65	0.937
20	23.55	0.0472	1.55	0.966

Table S2. Comparison of different adsorbents tested in the removal of MB.

Adsorbent	Maximum adsorption capacity ($mg \cdot g^{-1}$)	Reference
Clinoptilolite/chitosan/EDTA	44.84	1
Chitosan-gelatin@tin(IV) Tungstatophosphate	3.72	2
Chitosan/clay/Fe_2O_3	45.1	3
Chitosan/zeolite composite	24.5	4
Graphene-Fe_3O_4/calcium alginate	37.04	5
S-CNF	36.97	6
HNT sponges	45.59	7
CNCs	101.16	8
PD-CNCs	130.04	9
CNC-HNT-0.4	59.15	This work

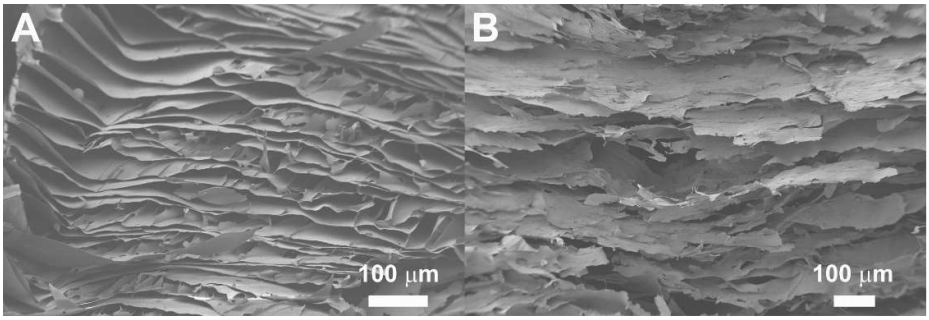

Fig. S17 SEM images for CNC-HNT sorbents (A) before and (B) after MB adsorption.

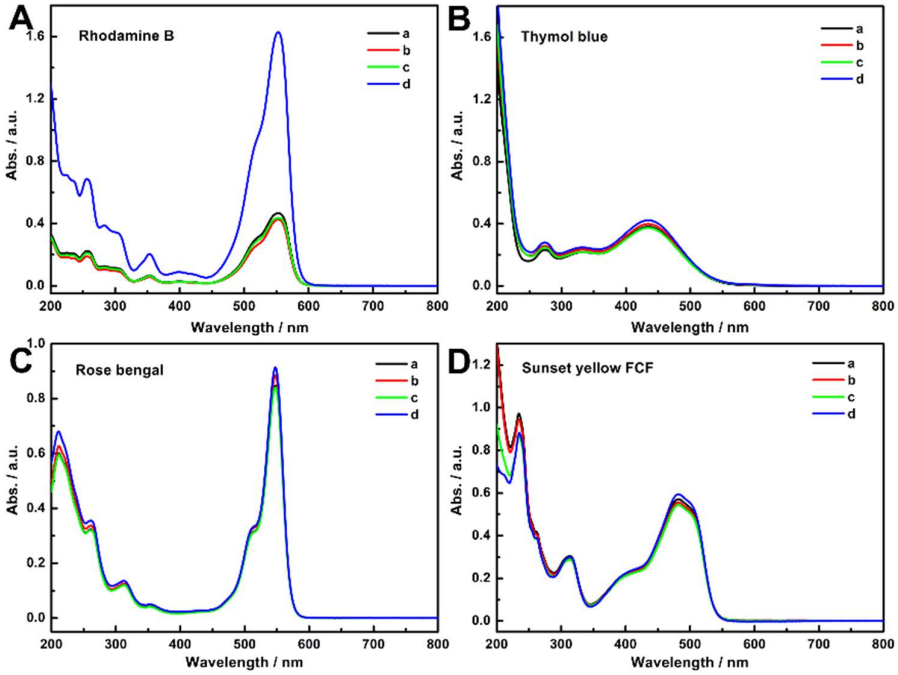

Fig. S18 UV-vis spectra of different types of dyes' solution after adsorption onto CNC-HNT-0.4. For each experiment, 10 mL of dye solution (10 mg·L^{-1}) was combined with 4 mg of CNC-HNT-0.4 and stirred for 360 min at room temperature. Then, UV-vis spectra were obtained to monitor the change in dye concentration in the solution. In each graph, trace a represents the original dye solution, and traces b-d show three independent adsorptive results. Note that thymol blue and sunset yellow FCF are anionic, rhodamine B is cationic, and rose bengal is neutral.

References

1. F. Aeenjan and V. Javanbakht, Methylene blue removal from aqueous solution by magnetic clinoptilolite/chitosan/EDTA nanocomposite, *Res. Chem. Intermed.,* **2018**, *44*, 1459–1483.
2. K. Kaur, R. Jindal and R. Tanwar, Chitosan–gelatin@tin (IV) tungstatophosphate nanocomposite ion exchanger: synthesis, characterization and applications in environmental remediation, *J. Polym. Environ.,* **2019**, *27*, 19–36.
3. D. W. Cho, B. H. Jeon, C. M. Chon, F. W. Schwartz, Y. Jeong and H. Song, Magnetic chitosan composite for adsorption of cationic and anionic dyes in aqueous solution, *J. Ind. Eng. Chem.,* **2015**, *28*, 60–66.
4. M. H. Dehghani, A. Dehghan, H. Alidadi, M. Dolatabadi, M. Mehrabpour and A. Converti, Removal of methylene blue dye from aqueous solutions by a new chitosan/zeolite composite from shrimp waste: kinetic and equilibrium study, *Korean J. Chem. Eng.,* **2017**, *34* (6), 1699–1707.
5. N. Song, X. L. Wu, S. Zhong, H. Lin and J. R. Chen, Biocompatible G-Fe_3O_4/CA nanocomposites for the removal of methylene blue, *J. Mol. Liq.,* **2015**, *212*, 63–69.
6. D. Wang, H. Yu, X. Fan, J. Gu, S. Ye, J. Yao and Q. Ni, High aspect ratio carboxylated cellulose nanofibers cross-linked to robust aerogels for superabsorption-flocculants: paving way from nanoscale to macroscale, *ACS Appl. Mater. Interfaces,* **2018**, *10*, 20755–20766.
7. T. Xu, F. Zheng, Z. Chen, Y. Ding, Z. Liang, Y. Liu, Z. Zhu and H. Fong, Halloysite nanotubes sponges with skeletons made of electrospun nanofibers as innovative dye adsorbent and catalyst support, *Chem. Eng. J.,* **2019**, *360*, 280–288.
8. X. He, K. B. Male, P. N. Nesterenko, D. Brabazon, B. Paull and J. H. T. Luong, Adsorption and desorption of methylene blue on porous carbon monoliths and nanocrystalline cellulose, *ACS Appl. Mater. Interfaces,* **2013**, *5*, 8796–8804.
9. N. Mohammed, H. Lian, M. S. Islam, M. Strong, Z. Shi, R. M. Berry, H. Y. Yu and K. C. Tam, Selective adsorption and separation of organic dyes using functionalized cellulose nanocrystals, *Chem. Eng. J.,* **2021**, *417*, 129237.